

## Role of $\text{HCO}_3^-$ and $\text{Cl}^-$ in the Pitting of 20CrMo Steel in simulated oil field environment

Bingying Wang\*, Ting Xin, Zhiwei Gao

School of Mechanical and Electrical Engineering, China University of Petroleum, Qingdao 266580, China

\*E-mail: [tdwby2004@126.com](mailto:tdwby2004@126.com)

Received: 3 May 2017 / Accepted: 17 June 2017 / Published: 12 July 2017

---

In this study, the effects of  $\text{HCO}_3^-$  and  $\text{Cl}^-$  concentrations on the pitting behavior of 20CrMo steel were investigated by potential polarization curve, electrochemical impedance spectroscopy and Mott-Schottky measurements. In addition, the concentrations of  $\text{HCO}_3^-$  and  $\text{Cl}^-$  in a simulated oil field environment were varied to investigate the interactions between  $\text{HCO}_3^-$  and  $\text{Cl}^-$ . The results indicated that with increasing  $\text{HCO}_3^-$  concentration, the passivation of  $\text{HCO}_3^-$  is enhanced, leading to the increase in the corrosion and pitting potentials and decrease in the number of defects in the passivation film as well as the corrosion current. With increasing  $\text{Cl}^-$  concentration, the erosion became severe, resulting in the loosening and breaking of the passivation film as well as the easy formation of holes. The  $[\text{Cl}^-]/[\text{HCO}_3^-]$  ratio exhibited a concentration threshold. The passivation of  $\text{HCO}_3^-$  played a dominant role below the critical value; the erosion effect of  $\text{Cl}^-$  is main role above the critical value and 20CrMo steel occurs dissolution.

---

**Keywords:** 20CrMo steel; pitting corrosion; polarization curve; passivation film

### 1. INTRODUCTION

As the majority of the oil fields have entered the extra-high water period, several corrosive media are present in the fluid, and the degree of mineralization is high. The localized corrosion of sucker rods has attracted considerable attraction. The high concentrations of  $\text{HCO}_3^-$  and  $\text{Cl}^-$  in the environment, main affect corrosion.

Li et al. [1] and Du et al. [2] have independently reported that the  $\text{HCO}_3^-$  in the environment plays a significant role in the corrosion behavior of pipeline steels. Li et al. [3] have investigated the corrosion behavior of X80 steel in  $\text{HCO}_3^-$  solution. The contact of pipeline steel with high pH soil, leads to the formation of a passivation film. Because of the presence of  $\text{HCO}_3^-$  in the soil, the effect of

$\text{HCO}_3^-$  on the corrosion of the pipeline steel is more complicated [4].  $\text{HCO}_3^-$  might form an oxide film with  $\text{Fe}^{2+}$  to prevent the anodic dissolution. On the contrary,  $\text{HCO}_3^-$  might break the corrosion product film, here by initiating pitting and stress corrosion cracking [5]. Hamadou et al. [6] have reported the correlation between the type of semiconductor and the pitting behavior of the passive film on carbon steel at different potentials.

The strong erosion by  $\text{Cl}^-$  can cause the localized rupture of the passivation film, leading to the initiation of pitting [7]. P. Marcus et al. [8] have reported that pitting result from the competitive adsorption of  $\text{Cl}^-$  and  $\text{OH}^-$  in solution. Cheng et al. [9] have pointed out that  $\text{Cl}^-$  leads to the occurrence of pitting as a result of the increase in the probability of localized rupture of the passivation film rather than the preventing of surface repassivation. Above a certain chloride threshold concentration, the passivation film on the reinforcing steel breaks down, inducing the pitting corrosion of steel [10-13]. Zuo Y et al. [14,15] have reported that  $\text{Cl}^-$  exerts a similar effect on the metastable pitting potential ( $E_m$ ) and pitting potential ( $E_b$ ) values of carbon steel and stainless steel.

When the  $[\text{Cl}^-]/[\text{OH}^-]$  ratio exceeds the threshold, the breakdown and repassivation of the passivation film at the local active site on rebars probably cause fluctuations in the potential and current [16]. The localized corrosion readily occurs in case the  $[\text{Cl}^-]/[\text{OH}^-]$  ratio exceeds 0.2–2 [17,18].

In the previous investigation, although several studies have been conducted to elucidate the pitting behavior of carbon steel in single- and double-ion systems and the relationship between the  $[\text{Cl}^-]/[\text{OH}^-]$  ratio and electrochemical corrosion, few studies have focused on the corrosion behavior of 20CrMo steel in simulated oil field environment. The corrosion mechanism and the interactions between  $\text{HCO}_3^-$  and  $\text{Cl}^-$  need to be investigated further. In this study, the effects of  $\text{Cl}^-$  and  $\text{HCO}_3^-$  on the electrochemical behavior of 20CrMo steel and the interaction between them were investigated by the potential polarization, electrochemical impedance spectroscopy, and Mott-Schottky curve. In addition, the relationship between the  $[\text{Cl}^-]/[\text{HCO}_3^-]$  ratio and the corrosion of 20CrMo Steel was studied.

## 2. EXPERIMENT

Specimens with dimensions of 10 mm×10 mm×2 mm were cut from a sheet of 20CrMo steel. All sides of the specimen surfaces were ground using a SiC emery paper down to 1000 gri. To prevent crevice corrosion, the samples were embedded in epoxy resin, leaving an area of 1 cm<sup>2</sup> exposed to solution prior to measurements. The exposed surface of the specimen was polished up to 1200 grit, cleaned in distilled water and degreased in methanol.

The base solution was 0.01 M  $\text{Na}_2\text{SO}_4$  + 0.01 M  $\text{Na}_2\text{CO}_3$ . To examine the effects of  $\text{Cl}^-$  and  $\text{HCO}_3^-$  on the pitting of 20CrMo steel,  $\text{NaCl}$  and  $\text{NaHCO}_3$  were added to the base solution to yield different  $\text{Cl}^-$  and  $\text{HCO}_3^-$  concentrations. All of the solutions were prepared from analytical-grade reagents and distilled water.

All the experiments were conducted using typical three-electrode electrochemical cells in the multi-ion solution. A saturated calomel electrode and a graphite rod was used as the reference and counter electrodes. The working electrodes were composed of 20CrMo steel.

First, the working electrode was immersed in a test solution for a certain time to reach a steady open-circuit potential. Next, polarization curves were obtained in a scanning potential range of -0.2 V to 2.0 V and at a scanning speed of  $0.166 \text{ mV}\cdot\text{s}^{-1}$ .

The impedance measurements were carried out in a frequency range of  $10^5 \text{ Hz}$  to  $10^{-2} \text{ Hz}$ , and the amplitude of the harmonic potential perturbation was 10mV. By the application of a stabilization potential of 0.5V for 60 min impedance plots were obtained.

Mott-Schottky measurements were carried out at a scanning potential was from -0.5 V to 1 V with a scanning rate of 40 mV/s.

### 3. RESULTS AND DISCUSSION

#### 3.1 Potentiodynamic polarization curves for various $\text{HCO}_3^-$ and $\text{Cl}^-$ concentrations

Table 1 shows the pH values in different  $\text{HCO}_3^-$  concentration solutions. With the change in  $\text{HCO}_3^-$  concentration from 0.01 M to 0.1 M, the pH values decrease from 9.94 to 8.97. The magnitude of the pH value is affected by the hydrolysis reaction of  $\text{HCO}_3^-$  and  $\text{CO}_3^{2-}$ . The following element reactions, reactions (1)-(2), are possible. With the increase in the concentration of  $\text{HCO}_3^-$ , the hydrolysis of  $\text{CO}_3^{2-}$  decreases. On the contrary, the hydrolysis of  $\text{HCO}_3^-$  increases. Because the hydrolytic degree of  $\text{CO}_3^{2-}$  is greater than the hydrolytic degree of  $\text{HCO}_3^-$ , the content of  $\text{OH}^-$  reduces. And the pH value decreases.

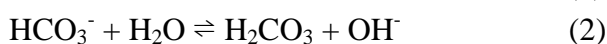
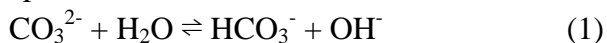


Fig.1 (a) shows the potentiodynamic polarization curves for 0.01-0.1 M solutions. In a 0.01 M  $\text{NaHCO}_3$  solution, active dissolution was observed on the 20CrMo steel surface. The  $\text{HCO}_3^-$  concentration of the solution is too low to form a passive film. The polarization curves exhibit a typical active-passive-transpassive characteristics [19] in 0.03-0.1 M  $\text{NaHCO}_3$  solutions. A current peak and a small passive region in the 0.03 M  $\text{NaHCO}_3$  solution are observed, suggesting that the surface iron matrix reacts with  $\text{HCO}_3^-$  to produce some iron compounds [20], these compounds are attached to the steel surface to form a short-lived and weak passive film. Two current peaks and a large steady passive region are observed in the 0.05 M  $\text{NaHCO}_3$  solution. The second peak current is considerably greater than the first peak current. The previously generated corrosion products are transformed to other corrosion products, leading to the formation of a stable passivation film. There is no current peak is observed before the steady passive region in the 0.1 M  $\text{NaHCO}_3$  solution. The pitting potentials increase rapidly with increasing  $\text{HCO}_3^-$  concentration in 0.03-0.1 M  $\text{NaHCO}_3$  solutions.

With the change in  $\text{HCO}_3^-$  concentration from 0.01 M to 0.1 M, the pH values decrease. As the pH value decreases, more stable and protective Cr oxides are enriched in the film while Fe oxides gradually decompose [21], providing the film higher corrosion resistance and less conductivity. At high pH, chromium ions become more soluble, whereas iron oxides are more stable. When the pH value drops, the chromium concentration within the surface film increases due to the tendency for higher stability of the Cr oxides. Higher content of Cr oxides in the film layer provides corrosion-

resistant steel more excellent passivity at lower pH value [22].

The shape of the polarization curves in Fig.1 (b) significantly changes with the addition of  $\text{Cl}^-$ , indicating that the corrosion mechanism of 20CrMo steel changes. The  $[\text{Cl}^-]/[\text{HCO}_3^-]$  ratio ranges from 0 to 2.5, the erosion of  $\text{Cl}^-$  sharply increases. The rate ranges from 2.5 to 5, the erosion of  $\text{Cl}^-$  increased slowly. The rate ranges from 5 to 10, and the erosion of  $\text{Cl}^-$  is basically stable. When the  $[\text{Cl}^-]/[\text{HCO}_3^-]$  ratio is 10, a tiny anode peak is still existed which indicates that the passivation of  $\text{HCO}_3^-$  is slightly stronger than the erosion of  $\text{Cl}^-$ .

As shown in Fig.1 (c) a slight passive trend is still observed on the steel surface with a  $[\text{Cl}^-]/[\text{HCO}_3^-]$  ratio of less than 20. At a ratio of greater than 33.3, active dissolution occurs at the surface. The threshold level of  $[\text{Cl}^-]/[\text{HCO}_3^-]$  for the passivation of 20CrMo steel is between 20 and 33.3.

Table 2 summarizes the data of potentiodynamic polarization curves. With the increase in the concentration of  $\text{HCO}_3^-$  solution with or without  $\text{Cl}^-$ , the  $E_{\text{corr}}$  values increase,  $i_{\text{corr}}$  values gradually decrease and  $E_b$  values increase. It can be seen that for 20CrMo steel in alkaline solutions, less alkalinity offers better conditions for a higher protective passive film forming. This phenomenon probably accounts for the increasing enrichment of more protective Cr species in the passive film when the pH drops [21]. As the pH decreases, the film thickness increases [23].

The passivation is enhanced with increasing  $\text{HCO}_3^-$  concentration. With increasing  $\text{Cl}^-$  concentration, the  $E_{\text{corr}}$  values decrease,  $i_{\text{corr}}$  values increase and  $E_b$  values decrease.  $\text{Cl}^-$  increases the rate of corrosion of 20CrMo steel. It can accelerate the initiation of pitting.

Table 3 shows  $E_{\text{corr}}$  and  $i_{\text{corr}}$  values for different  $[\text{Cl}^-]/[\text{HCO}_3^-]$  values. When the  $[\text{Cl}^-]/[\text{HCO}_3^-]$  ratio ranges from 2.5 to 10, the  $E_{\text{corr}}$  values decrease rapidly in an exponential function, with easier corrosion. The rate ranges from 10 to 100, and the  $E_{\text{corr}}$  values are stable which shows that the erosion effect of  $\text{Cl}^-$  is basically equal. Fig.2 (a) shows that the relationship between  $E_{\text{corr}}$  and the  $[\text{Cl}^-]/[\text{HCO}_3^-]$  rate can be described by the follow equation (3):

$$Y = -0.7196 + 0.4690 \times 0.6003^x \quad (3)$$

When the  $[\text{Cl}^-]/[\text{HCO}_3^-]$  ratio ranges from 2.5 to 33.3, the  $i_{\text{corr}}$  values rapidly increase, indicating that the corrosion rate of 20CrMo steel increases. The ratio ranges from 33.3 to 100, and the  $i_{\text{corr}}$  values slowly increase. Fig.2 (b) shows the relationship between  $i_{\text{corr}}$  and the  $[\text{Cl}^-]/[\text{HCO}_3^-]$  ratio. It is described by equation (4):

$$Y = 1.0528 \times 10^{-5} - 4.37752 \times 10^{-6} \times 0.97872^x \quad (4)$$

The effects of the  $[\text{Cl}^-]/[\text{HCO}_3^-]$  ratio on  $E_{\text{corr}}$  and  $i_{\text{corr}}$  are not synchronous. The  $[\text{Cl}^-]/[\text{HCO}_3^-]$  ratio ranges from 2.5 to 10,  $E_{\text{corr}}$  is more sensitive than  $i_{\text{corr}}$ . The  $[\text{Cl}^-]/[\text{HCO}_3^-]$  ratio ranges from 2.5 to 100,  $i_{\text{corr}}$  is more sensitive than  $E_{\text{corr}}$ . Finally, the values of  $E_{\text{corr}}$  and  $i_{\text{corr}}$  are stable.

**Table 1.** The pH values of solutions

$\text{HCO}_3^-$ concentration	0.01 M	0.03 M	0.05 M	0.1 M
pH value	9.94	9.53	9.30	8.97

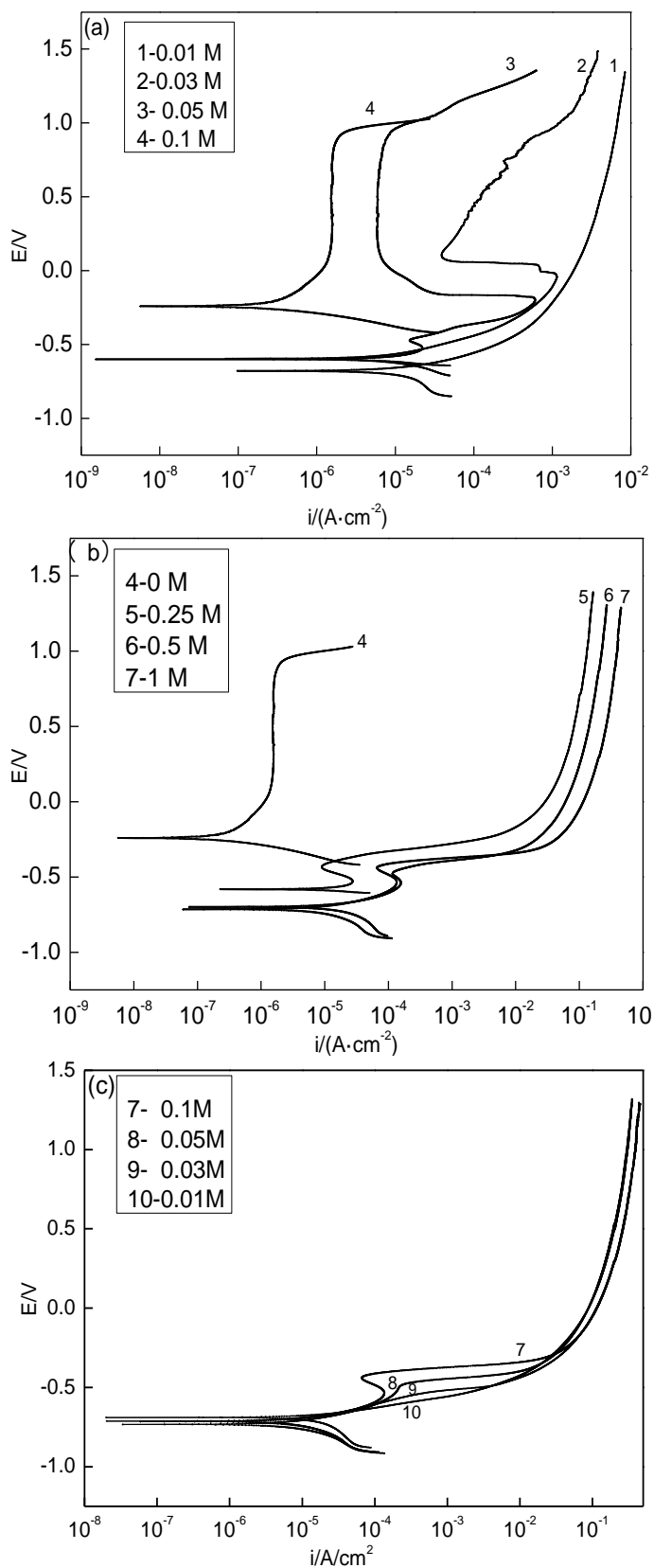


**Figure 1.** Potentiodynamic polarization curves for various  $\text{HCO}_3^-$  and  $\text{Cl}^-$  concentrations. (a) Different concentrations of  $\text{NaHCO}_3$  (b) 0.1 M  $\text{NaHCO}_3$ , different concentrations of  $\text{NaCl}$  (c) 1 M  $\text{NaCl}$ , different concentrations of  $\text{NaHCO}_3$

**Table 2.** Data of potentiodynamic polarization curves

Solution	$E_{corr}/V$	$i_{corr}/(A \cdot cm^{-2})$	$Eb/V$
1	-0.6927	$8.9572 \times 10^{-6}$	/
2	-0.6065	$7.5008 \times 10^{-6}$	0.1306
3	-0.6046	$5.6465 \times 10^{-6}$	0.8898
4	-0.2507	$2.1704 \times 10^{-7}$	0.8920
5	-0.5882	$6.4339 \times 10^{-6}$	-0.4231
6	-0.6830	$6.7985 \times 10^{-6}$	-0.4695
7	-0.7148	$6.9883 \times 10^{-6}$	-0.4344
8	-0.7189	$7.4078 \times 10^{-6}$	/
9	-0.7196	$8.7196 \times 10^{-6}$	/
10	-0.7203	$1.0039 \times 10^{-5}$	/

**Table 3.**  $E_{corr}$  and  $i_{corr}$  values for different  $[Cl^-]/[HCO_3^-]$  values.

$[Cl^-]/[HCO_3^-]$	2.5	5	10	20	33.3	100
$E_{corr}$ values	$1.0039 \times 10^{-5}$	$8.7196 \times 10^{-6}$	$8.7196 \times 10^{-6}$	$6.9883 \times 10^{-6}$	$6.7985 \times 10^{-6}$	$6.4339 \times 10^{-6}$
$i_{corr}$ values	-0.5882	-0.6830	-0.7148	-0.7189	-0.7196	-0.7203

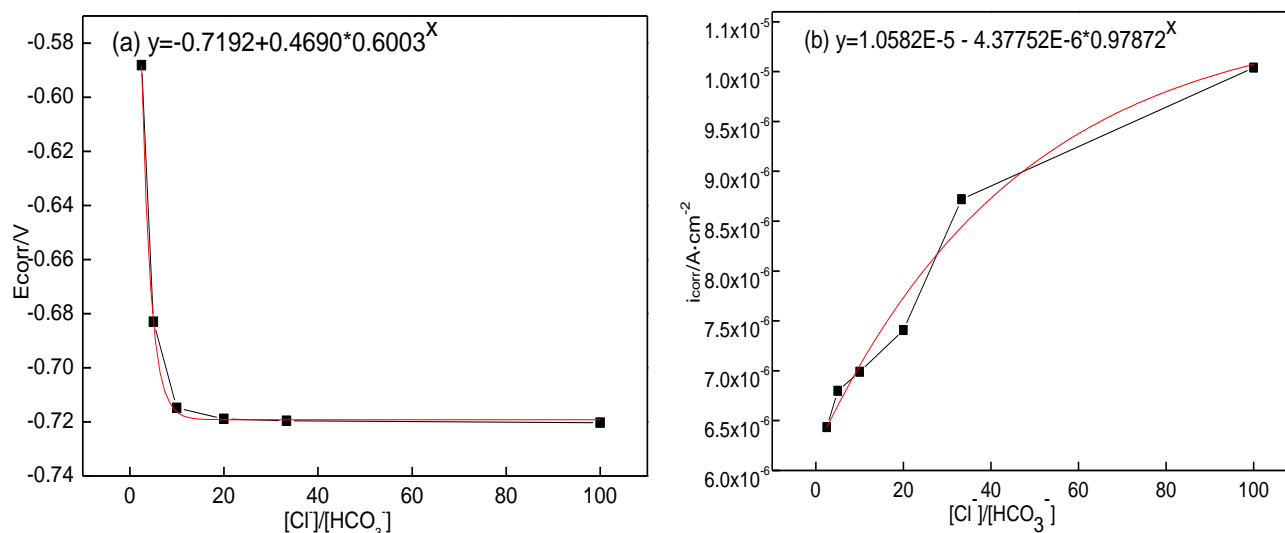


**Figure 2.**  $E_{corr}$  and  $i_{corr}$  values for different  $[Cl^-]/[HCO_3^-]$  values. (a)  $E_{corr}$  (b)  $i_{corr}$

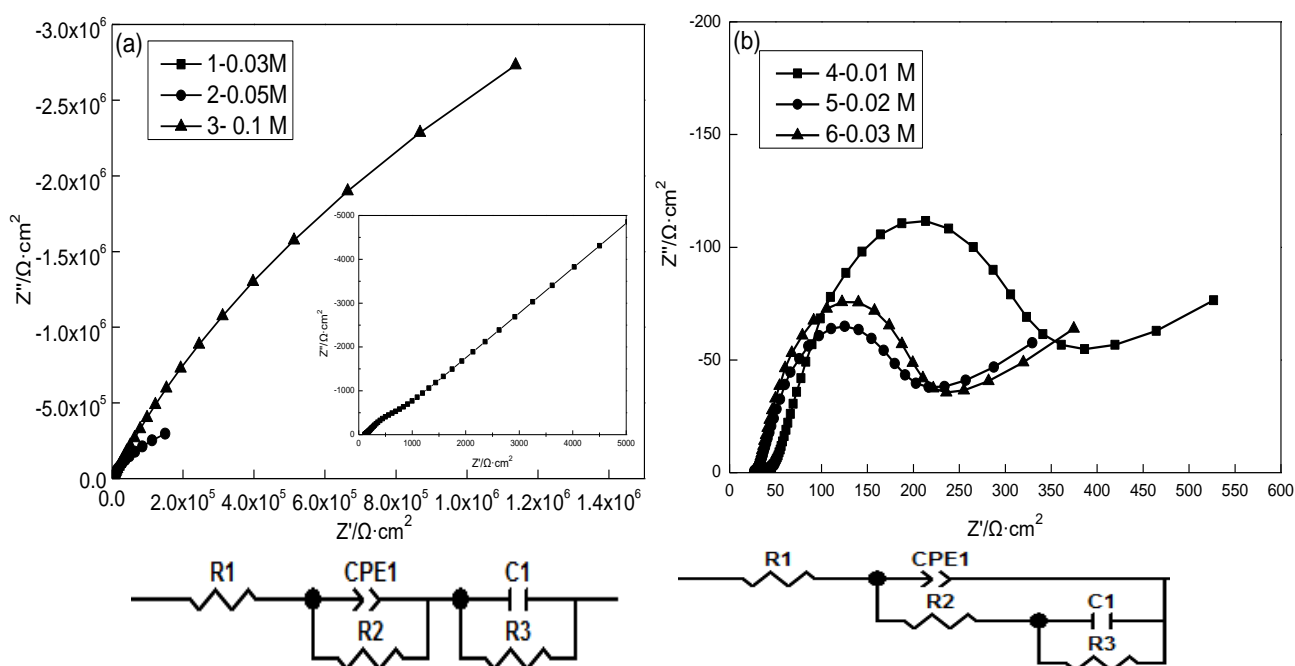
### 3.2 Electrochemical impedance spectroscopy behaviors

As seen in Fig.3, R1 represents the resistance of solution. R2 and CPE1 represent the resistance and capacity of the passivation film, respectively. R3 and C1 represent the resistance and capacity of the electrical double layer, respectively. The Warburg impedance exists in the electrochemical process.

Fig.3 (a) shows the Nyquist plots and equivalent circuits for different  $HCO_3^-$  concentrations. When  $HCO_3^-$  concentration is 0.03 M, there are one piece of capacitive impedance arc at high frequency and one piece of warburg impedance at low frequency. The capacitive impedance arc

represents that the passivation film is complete. The Warburg impedance shows that the passive film is broken. The corrosion control system transforms from a charge control system to a diffusion control system. With the change in  $\text{HCO}_3^-$  concentration from 0.05 M to 0.1 M, there is a single capacitive impedance arc. With increasing the pH value, the radius of the capacitive impedance arc increases, and the passivation is stronger. The capacitance arc magnitude and overall impedance are even larger at pH 8.97, indicating the film formed at lower pH exhibits more protective behavior.

Table 4 summarizes the fitting data for the equivalent circuits. With the increase in the concentration of  $\text{HCO}_3^-$  solution from 0.03 M to 0.1 M, R1 values increase from  $115.7 \Omega \cdot \text{cm}^2$  to  $754 \Omega \cdot \text{cm}^2$ , and R3 values gradually increase from  $1.203 \times 10^5 \Omega \cdot \text{cm}^2$  to  $1.603 \times 10^7 \Omega \cdot \text{cm}^2$ . In addition, the CPE1 values decrease from  $4.608 \times 10^{-4} \Omega^{-1} \cdot \text{cm}^{-2} \cdot \text{S}^{-n}$  to  $3.489 \times 10^{-6} \Omega^{-1} \cdot \text{cm}^{-2} \cdot \text{S}^{-n}$ , and C1 values decrease  $2.876 \times 10^{-4} \Omega^{-1} \cdot \text{cm}^{-2} \cdot \text{S}^{-n}$  to  $3.798 \times 10^{-6} \Omega^{-1} \cdot \text{cm}^{-2} \cdot \text{S}^{-n}$ . With increasing  $\text{HCO}_3^-$  concentration, the resistance of the solution increases, and the movement of ions becomes more difficult. At a constant applied voltage, the current density of the passive film decreases, and the corrosion rate becomes slower.



(a) different  $\text{NaHCO}_3$  concentrations (b) 0.1 M  $\text{NaHCO}_3$ , different  $\text{NaCl}$  concentrations

**Figure 3.** The Nyquist plots and the equivalent circuits for different concentrations of  $\text{NaHCO}_3 + \text{NaCl}$  solutions

The concentration of  $\text{NaCl}$  solution changes from 0.01 M to 0.03 M in Fig.3 (b). A high-frequency capacitive impedance arc and low-frequency Warburg impedance are observed in all of the Nyquist plots. Warburg impedance exists for a wide range of  $\text{Cl}^-$  concentration, this implies that the corrosion processes are diffusion controlled whether in low or high chloride content solutions [24]. The radius of the semicircle gradually decreases, and the shape of the electrochemical impedance spectrum exhibits noticeable changes with increasing  $\text{Cl}^-$  concentration.  $\text{Cl}^-$  accumulates at the steel interface

which can cause the initiation and propagation of pits. After a pit is initiated, it grows both vertically and horizontally. After several minutes, a small hole is formed. The dissolution of metal in the initiation process produces anodic ions around the holes, resulting in the migration of chloride ions. The chloride ions diffuses in horizontal direction, leading to the final formation of a stable pit [25].

With increasing Cl<sup>-</sup> solution concentration from 0.01M to 0.03M, R1 values decrease from 51.54 Ω•cm<sup>2</sup> to 31.16 Ω•cm<sup>2</sup>, R2 values decrease from 137.1 Ω•cm<sup>2</sup> to 84.92 Ω•cm<sup>2</sup>, R3 values decrease from 217.6 Ω•cm<sup>2</sup> to 128.2 Ω•cm<sup>2</sup>. While CPE1 values increase from 9.388×10<sup>-3</sup> Ω<sup>-1</sup>•cm<sup>-2</sup>•S<sup>-n</sup> to 0.0144 Ω<sup>-1</sup>•cm<sup>-2</sup>•S<sup>-n</sup>, C1 values increase from 7.256×10<sup>-3</sup> Ω<sup>-1</sup>•cm<sup>-2</sup>•S<sup>-n</sup> to 0.0134 Ω<sup>-1</sup>•cm<sup>-2</sup>•S<sup>-n</sup>. With the addition of Cl<sup>-</sup>, the corrosion mechanism of 20CrMo steel has changed. The passivation film exhibits a dynamic equilibrium state. With the presence of Cl<sup>-</sup> in solution, the dynamic equilibrium of the passive film is destroyed, the dissolution rate of passive film is greater than the growth rate, and penetrating fracture occurs on the passive film. Cl<sup>-</sup> not only destroys the passive film and leads to the occurrence of pitting corrosion, but also promotes the growth of pitting corrosion due to the concentration of Cl<sup>-</sup> inside the pit [26].

**Table 4.** Values of equivalent circuits

Solutio n	R <sub>1</sub> Ω•cm <sup>2</sup>	R <sub>2</sub> Ω•cm <sup>2</sup>	C <sub>1</sub> Ω <sup>-1</sup> •cm <sup>-2</sup> •S <sup>-n</sup>	R <sub>3</sub> Ω•cm <sup>2</sup>	CPE <sub>1</sub> Ω <sup>-1</sup> •cm <sup>-2</sup> •S <sup>-n</sup>	n
1	115.7	166.3	2.876×10 <sup>-4</sup>	1.203×10 <sup>5</sup>	4.608×10 <sup>-4</sup>	0.515
2	151.4	83.04	1.226×10 <sup>-5</sup>	1.228×10 <sup>6</sup>	3.070×10 <sup>-5</sup>	0.874
3	754	26.45	3.798×10 <sup>-6</sup>	1.603×10 <sup>7</sup>	3.489×10 <sup>-6</sup>	0.864
4	51.54	137.1	7.256×10 <sup>-3</sup>	217.6	9.388×10 <sup>-3</sup>	0.481
5	32.93	84.49	-0.4231	144.2	0.0132	0.519
6	31.16	84.92	-0.4695	128.2	0.0144	0.514

### 3.3 Semiconducting nature of the passive film

A linear relationship between capacitance and the applied potential can be expressed by the Mott–Schottky equation .

$$C^{-2} = \frac{2}{\epsilon\epsilon_0 e N_D} \left( E - E_{FB} - \frac{kT}{e} \right) \quad \text{n-type semiconductor}$$

$$C^{-2} = -\frac{2}{\epsilon\epsilon_0 e N_A} \left( E - E_{FB} - \frac{kT}{e} \right) \quad \text{p-type semiconductor}$$

Where ε is the dielectric constant of the passive film, ε<sub>0</sub> is the permittivity of free space (8.854×10<sup>-14</sup> F/cm), e is the electron charge (1.602 × 10<sup>-19</sup>C), N<sub>D</sub> and N<sub>A</sub> are the donor and acceptor densities. E<sub>FB</sub> is the flat-band potential, T is the absolute temperature (298K), and k is the Boltzmann constant (1.38×10<sup>-23</sup>J/K). The dielectric constant of the passive film on the stainless steels is 15.6 [27]. N<sub>D</sub> and N<sub>A</sub> can be determined from the slope of the experimental C<sup>-2</sup> vs. applied potential.

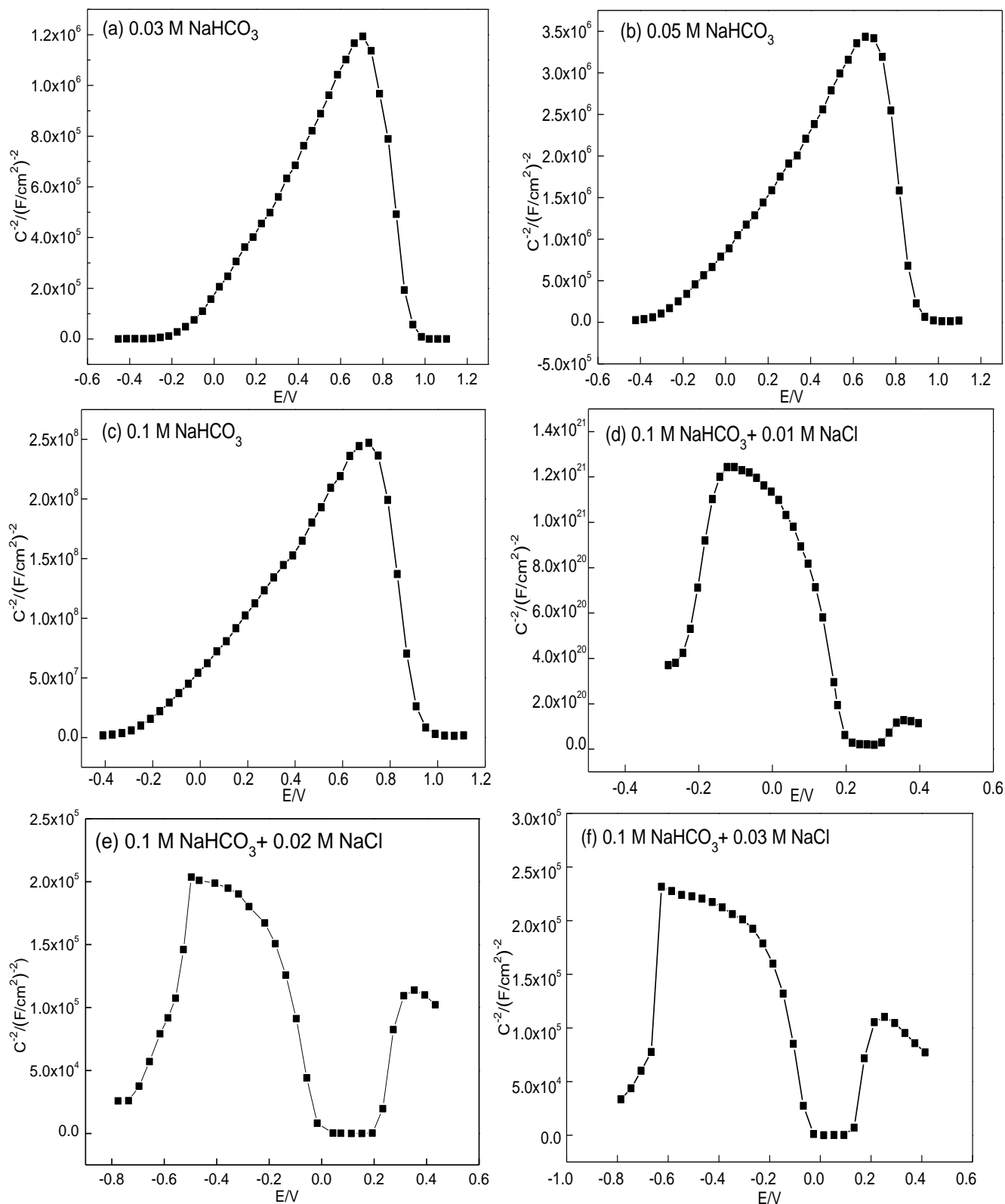


**Figure 4.** The Mott-Schottky plots for different concentrations  $NaHCO_3$  and  $NaCl$  solutions

Fig.4 shows the Mott–Schottky plots at different concentrations of  $NaHCO_3$  and  $NaCl$  solutions. Two lines with positive and negative slopes, respectively, characterized by different capacitance

behaviors and separated by peak potentials in all the Mott–Schottky plots, are observed. With the increase in the scanning potential, the presence of a peak region is observed, relates to the excess charge present on the oxide surface. The positive region of the straight line is indicative of the n-type semiconducting behavior (iron oxide), while the negative potential region of the straight line indicates the p-type semiconducting behavior (chromium oxide) of the passive film [28].

With the increase in the  $\text{NaHCO}_3$  solution concentration changes from 0.03 M to 0.05 M and 0.1 M, the peak potentials are 0.70V, 0.69V, and 0.71V, respectively. The  $N_D$  and  $N_A$  values decrease with increasing  $\text{HCO}_3^-$  concentration. Lower values are observed in the alloy with the highest  $\text{HCO}_3^-$  concentration. The donors or acceptors in the semiconducting passivation film constitute defects, e.g., cation and anion vacancies. The concentration of electronic defects decreases with pH and that the films formed at highest pH present the highest density of donors, indicating a more conductive behavior. Generally, the rupture of the metal passivation film and the initiation of the pitting generally occur at the defective locations within the passivation film. The internal structure in the passivation film is more stable with few defects [29].

With the increase in the NaCl solution concentration changes from 0.03 M to 0.05 M and 0.1 M, the peak potentials are 0.70V, 0.69V, and 0.71V, respectively. With the increase in the  $\text{Cl}^-$  concentration, the peak potential become more negative. The  $\text{Cl}^-$  from the solution is adsorbed on the passivation film surface, hence, the concentration of negative charge on the surface increases. With increasing  $\text{Cl}^-$  concentration, the  $N_D$  and  $N_A$  values increase and defects increase.

#### 4. CONCLUSION

(1)With the increase in the  $\text{HCO}_3^-$  concentration in the simulated oil field environment, the .resistance to pitting corrosion and transpassive potential of 20CrMo steel increased. The resistance to pitting corrosion and transpassive potential decreased with increasing  $\text{Cl}^-$  concentration.  $\text{Cl}^-$  can decrease the pitting potential and improve the dissolution rate of the passivation film.

(2)The  $\text{HCO}_3^-$  and  $\text{Cl}^-$  concentrations affect the semiconducting nature of the passive film. Capacitance studies revealed the existence of n-and p-type semiconductors. The  $N_D$  and  $N_A$  values decreased with increasing  $\text{HCO}_3^-$  concentration. The opposite side, the  $N_D$  and  $N_A$  values, increased with increasing  $\text{Cl}^-$  concentration. These results indicated that the oxide layers of the passive film are modified by  $\text{HCO}_3^-$  and  $\text{Cl}^-$ .

(3)The ratio of  $[\text{Cl}^-]/[\text{HCO}_3^-]$  in the multi-ion mixed system is closely related to the corrosion of 20CrMo steel. When the  $[\text{Cl}^-]/[\text{HCO}_3^-]$  ratio is less than 20, the passivation of  $\text{HCO}_3^-$  is dominant. On the contrary, when the  $[\text{Cl}^-]/[\text{HCO}_3^-]$  ratio is greater than 20, the active dissolution of 20CrMo steel occurs. The  $[\text{Cl}^-]/[\text{HCO}_3^-]$  ratio ranged from 0.1 to 0.2, and the erosion of  $\text{Cl}^-$  in the passivation film increases rapidly. The  $[\text{Cl}^-]/[\text{HCO}_3^-]$  ratio ranged from 0.2 to 0.3, and the erosion of  $\text{Cl}^-$  slowly increased.

#### References

1. M.C. Li, Y.F Cheng, *Electrochim. Acta.*, 53(2008)2831.

2. C.W. Du, X.G. Li, X. Chen, *Acta Metall. Sin.*, 21(2008)235.
3. D.G. Li, Y.R. Feng, Z.Q. Bai, *Appl. Surf. Sci.*, 254(2008)2837.
4. J.G. Gonzalez-Rodriguez, M.G. Casales, V.M. Salinas-Bravo, *Corrosion (Houston, Tx, U.S.)*, 58(2002)584.
5. Z. Lu, C. Huang, D. Huang, *Corros. Sci.*, 48(2006)3049.
6. L. Hamadou, A. Kadri, N. Benbrahim, *Appl. Surf. Sci.*, 252(2005)1510.
7. D.G. Li, Y.R. Feng, Z.Q. Bai, *Electrochim. Acta.*, 52(2007)7877.
8. P. Marcus, V. Maurice, H.H. Strehblow, *Corros. Sci.*, 50(2008)2698.
9. Y.F. Cheng, M. Wilmott, J.L. Luo, *Appl. Surf. Sci.*, 152(1999)161.
10. S.M.A.E. Haleem, S.A.E. Wanees, A. Bahgat, *Corros. Sci.*, 75(2013)1.
11. S.M.A.E. Haleem, S.A.E. Wanees, E.E.A.E. Aal, *Corros. Sci.*, 52(2010)1675.
12. Z.H. Dong, S. Wei, A.Z. Guo, *Electrochim. Acta.*, 56(2011)5890.
13. M. Liu, X. Cheng, X. Li, *Constr. Build. Mater.*, 93(2015)884.
14. Y. Zuo, H. Wang, J. Zhao, *Corros. Sci.*, 44(2002)13.
15. Y. Zuo, H. Wang, J. Xiong, *Corros. Sci.*, 44(2002)25.
16. G.F. Qiao, J.P. Ou, *Electrochim. Acta.*, 52(2007)8008.
17. K.Y. Ann, H.W. Song, *Corros. Sci.*, 49(2007)4113.
18. V.T. Ngala, C.L. Paga, M.M. Paga, *Mater. Corros.*, 55(2004)511.
19. Z. Lu, C. Huang, D. Huang, *Corros. Sci.*, 48(2006)3049.
20. J.M. Blengino, M. Keddam, J.P. Labbe, *Cheminform.*, 26(1995)621.
21. L. Freire, M.J. Carmezim, M.G.S. Ferreira, *Electrochim Acta.*, 55(2010)6174.
22. Z.Y. Ai, J.Y. Jiang, W. Sun, *Appl Surf. Sci.*, 389(2016)1126.
23. C.O.A. Olsson, D. Landolt, *Electrochim Acta.*, 48(2003)1093.
24. Y.F. Wang, G.G. Cheng, *Appl. Surf. Sci.*, 349(2015) 746.
25. Y.F. Wang, G.G. Cheng, Y. Li, *Corros. Sci.*, 111(2016) 508.
26. L.B. Niu, K. Nakada, *Corros. Sci.*, 96(2015)171.
27. C.A. Gervasi, M.E. Folquer, A.E. Vallejo, *Electrochim. Acta.*, 50(2005)1113.
28. S. Fujimoto, H. Tsuchiya, *Corros. Sci.*, 49(2007)195.
29. S. Ningshen, U.K. Mudali, V.K. Mittal, *Corros. Sci.*, 49(2007)481.

© 2017 The Authors. Published by ESG ([www.electrochemsci.org](http://www.electrochemsci.org)). This article is an open access article distributed under the terms and conditions of the Creative Commons Attribution license (<http://creativecommons.org/licenses/by/4.0/>).